Structure of liquid ethylene glycol: A molecular dynamics simulation study with different force fields

L. Saiz[a)]
Center for Molecular Modeling, University of Pennsylvania, 231 South 34th Street, Philadelphia, Pennsylvania 19104-6323

J. A. Padró
Universitat de Barcelona, Departament de Física Fonamental, Diagonal 647, E-08028 Barcelona, Spain

E. Guàrdia
Universitat Politècnica de Catalunya, Sor Eulàlia D'Anzizu, Campus Nord, Mòdul B4-B5, E-08034 Barcelona, Spain

(Received 4 February 2000; accepted 20 November 2000)

The structure of liquid ethylene glycol at room temperature is examined by performing molecular dynamics (MD) simulation studies for several different liquid phase force fields. We compare the properties obtained and analyze the differences which arise from the use of these models. A thorough study of molecular conformation and intermolecular structure for the different potential models is carried out given that three of the studied force fields have the same intermolecular parameters and different intramolecular interactions. In addition, the effect of molecular shape on the intermolecular structure is discussed. Due to the important role played by the highly directional forces occurring in hydrogen bonded systems, in their intermolecular structure and in the macroscopic properties of the system, we pay special attention to the analysis of the features of the hydrogen bonding patterns present in the liquid. Revealing an overall agreement with the available structural experimental data, the results obtained show that, for the simulated models, the intermolecular structure is rather similar. The dynamics of the system is studied through the self-diffusion coefficients and, in contrast to the structural properties, the results obtained for the distinct models are quite different. © *2001 American Institute of Physics.*
[DOI: 10.1063/1.1340605]

I. INTRODUCTION

Water is the most extensively studied solvent. However, it is surprising that considerably less attention has been devoted to the investigation of systems which in some way may be viewed as being similar to water. Ethylene glycol (EG) is one of the simplest polar molecules with internal degrees of freedom which may be regarded as a water analogue. This alcohol, in principle, can form three-dimensional networks of hydrogen bonded molecules since each molecule has two proton donor hydroxyl groups and two oxygen atoms that can act as proton acceptors in hydrogen bonds (HBs). Furthermore, since one can imagine the EG molecule as two methanol molecules linked by the methyl groups and because each methanol molecule participates in two hydrogen bonds on average in the liquid phase,[1,2] then providing the two subunits behave independently, one will expect a mean number of four hydrogen bonds per molecule. Therefore, both EG and liquid water have four HBs per molecule. As a matter of fact, a preliminary computer simulation study of the hydrogen bonding structure[2] of EG showed that this picture is likely to be found in the liquid. In addition, EG has one of the lowest ratios of weakly polar groups (methylene or methyl groups) vs polar groups (hydroxyl groups) in alcohols. Hence, the properties of this system will be dominated by hydrogen bonding interactions. In this regard, one might expect a behavior for EG closer to that of water than to that of better studied alcohols, such as alkanols.[1–5] The hydrogen bonding pattern in water consists of tetrahedral three-dimensional structures[1,2] of interacting molecules. Contrarily, in short monohydric alcohols, the structure is formed mainly by linear winding chains of hydrogen bonded molecules.[1–5] An additional effect expected in liquid EG is the possible competition between intermolecular and intramolecular interactions (hydrogen bonds). This competition is not present either in water or in alkanols because only intermolecular HBs can be formed in those cases. Although both substances (EG and water) present three-dimensional hydrogen bonded structures which extend the entire volume and both have four nearest-neighbors on average, the outstanding properties of water conferred by the peculiar characteristics (topology) of the hydrogen bonded network, such as the density maximum exhibited by water upon increasing temperature, cannot be displayed by EG or any other alcohol. Other features, however, such as the temporal evolution of the HBs, which at short times may be related to the corresponding hydrogen bonding pattern,[2] have been found to be similar for liquid EG and water. For instance, at short times, the linear hydrogen bonded chains of ethanol and methanol

[a)]Electronic mail: leonor@cmm.chem.upenn.edu

are more stable than the three-dimensional hydrogen bonded networks of ethylene glycol, glycerol, and water.[2]

Besides its theoretical interest, ethylene glycol as a solvent has many applications especially as a cryogenic liquid, like other members of the family of systems with multiple hydroxyl groups. Thus, aqueous solutions of EG are found in a glassy state, preventing the crystallization of ice below the freezing temperature of water. What makes this substance superior to other polyols is that lower concentrations of EG are needed to obtain similar results. This lowers the toxicity, which is of crucial importance in cryopreservation of living cells and tissues. Another aspect of this solvent relevant to its use in biology is the prevention of denaturalization of proteins, which adopt a more ordered structure in polyol solvents or aqueous polyol solutions.

Computer simulations provide a suitable tool to analyze the liquid properties from an atomic level and offer a direct connection between the microscopic details of the system and the macroscopic properties of experimental interest. In these atomistic studies, effective potentials are commonly used. Several force field models for liquid EG have been proposed in the literature. Computer simulations of ethylene glycol solutions in water,[6–13] in xenon,[7,8] or in carbon tetrachloride[12,13] have been carried out. The Monte Carlo (MC) simulation method[9–11] as well as molecular dynamics (MD)[6–8,12,13] have been used to study ethylene glycol solutions. In addition, Langevin dynamics have been applied to probe these systems.[6] Other methods such as umbrella sampling have been used in MD simulations for an aqueous solution of EG and for EG in carbon tetrachloride.[12,13] Nevertheless, no simulations of the pure solvent have been performed to date, apart from a comparative study[2] of hydrogen bonding in several liquid alcohols and water, where a preliminary hydrogen bonding analysis with one force field was presented. Although the proposed potential models are quite different, little effort has been devoted to the investigation of the effects of their differences on the static and dynamic properties of this system. It would be desirable thus to compare them and relate the different characteristics to differences on the properties for the proposed potentials in order to choose the one which gives the best agreement with the available experimental data.[14–40]

It is worth noting that the ethylene glycol molecule, whose chemical formula is $H–O–CH_2–CH_2–O–H$, has three torsional internal degrees of freedom. Therefore, at least 27 different conformers are stable for this molecule. Due to this fact, there is still some uncertainty about its equilibrium conformation, despite the large amount of experimental measurements and *ab initio* calculations for the gas phase. Depending on the energy difference among them, the ethylene glycol molecule could exist in either a *gauche* or a *trans* conformation or in a mixture of both (depending on temperature and the physical state). Furthermore, depending on the energy barrier between the different minima, the molecules will be more or less flexible from a dynamical point of view.[41]

The aim of this study is to probe the structure of liquid ethylene glycol by means of an MD simulation study. Besides this main purpose, we devote some effort to investigating the suitability of the existing potential models to perform realistic simulations of the liquid phase. Similarly, the effect of the different force fields in the studied properties is addressed. Here, we have focused on the static properties and only results for the self-diffusion coefficient are shown. However, a comparative analysis of the dynamics of liquid ethylene glycol for several force field models will be presented in a forthcoming publication.

We have organized this article as follows. The details of the molecular and force field models are reported in Secs. II A, and II B, whereas those of the molecular dynamics simulations are gathered in Sec. II C. In Sec. III A, the molecular conformation in the liquid is presented. The analysis of the intermolecular radial distribution functions and the orientational correlations of the molecular dipoles is summarized in Sec. III B. The results obtained for the structure are compared to neutron diffraction experimental data in Sec. III C. Section III D is devoted to the hydrogen bonding statistics. Some aspects of the dynamics, specifically the self-diffusion coefficients are presented in Sec. III E. Finally, we conclude by summarizing the main results obtained in this work.

II. COMPUTER SIMULATION DETAILS

A. Molecular model

The molecular model used throughout this article for all the force fields considered was proposed by Jorgensen in Ref. 42 for simulations of liquid alcohols. In this model, each ethylene glycol molecule is modeled using a united atom approximation. An EG molecule consisted of six interaction sites, i.e., the hydrogen atoms of the hydroxyl groups (H_O), the oxygen atoms (O), and the methylene (CH_2, termed Me) groups, which were considered as single interaction sites with their centers located at the position of the carbon atoms. In the united atom approach, the hydrogen atoms of the methylene groups are not explicitly considered; they are taken into account implicitly in the parameters. In Fig. 1(a), a sketch of an ethylene glycol molecule in this representation is shown.

Bond lengths and bond angles were kept fixed during the simulations and only torsions about the Me−Me central bond and about the Me−O bonds were allowed. Hence, there are three different dihedral angles for motions about the Me−Me central bond and the two Me−O bonds (Me−O and O−Me) for ethylene glycol.

B. Potential model

In this work, we studied four different force fields, namely, J, JMOD, WP and HTN. These potential models are based on those due to Jorgensen[42] (J and JMOD), Widmalm and Pastor[6] (WP), which is in turn derived from Jorgensen's potentials, and Hayashi, Tanaka, and Nakanishi[7,8] (HTN). The J model is a generalization of the transferable optimized potentials for liquid simulations (OPLS) model proposed by Jorgensen in Ref. 42 for simulations of liquid alkanols. Jorgensen[42] found that the OPLS model reproduces the structure and thermodynamic properties of a series of liquid alkanols. The OPLS model also gives[3,4] (at least for liquid

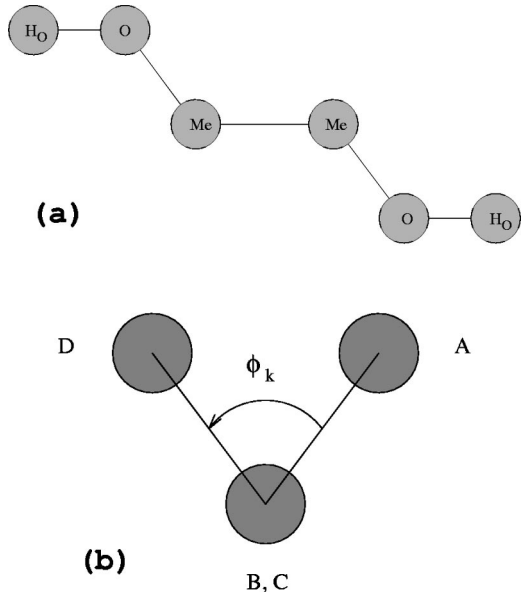

FIG. 1. (a) EG molecule as represented in the molecular model used in the MD simulations. $\phi_{\mathrm{Me-O}}$, $\phi_{\mathrm{Me-Me}}$, and $\phi_{\mathrm{O-Me}}$ are displayed in *trans* configurations. (b) Definition of the dihedral angle, ϕ_k. The figure shows the atoms involved in the calculation of the dihedral angle, ϕ_k, as viewed along the considered bond. *A* and *B* would be located underneath the plane of the paper whereas *C* and *D* would be located above it.

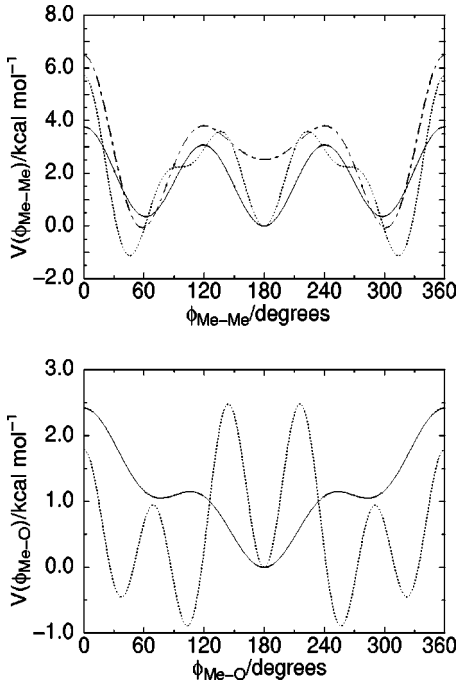

FIG. 2. Torsional energy function for rotations which involve the $\phi_{\mathrm{Me-Me}}$ (top) and the $\phi_{\mathrm{Me-O}}$ (bottom) dihedral angles for the four ethylene glycol models. Symbols are J and JMOD (full line), WP (dot-dashed line), and HTN (dotted line). Note that the torsional energy function corresponding to $\phi_{\mathrm{Me-O}}$ is identical for J, JMOD, and WP models whereas the one corresponding to $\phi_{\mathrm{Me-Me}}$ is coincident for J and JMOD models.

ethanol) a dependence of the dynamics of these systems on temperature, which is in good agreement with experimental data. The use of this model, which was optimized for liquid alkanols, to simulate the properties of liquid ethylene glycol is actually the idea behind the transferable models. The force field (WP) proposed by Widmalm and Pastor in Ref. 6 is also based on the OPLS force field. In their work, the authors modified certain aspects of the OPLS, specifically they basically introduced a different torsional potential to describe motions about the central C–C bonds, which was specific for dihydric alcohols similar to EG. In this article, we present a new hybrid model, JMOD. In the JMOD model, all potential functions and their parameters are the same as in the WP model with the exception of the torsional potential for motions about the central bond. In this case, we simply used the one proposed by Jorgensen.[42] Although the introduction of models with hybrid interactions, such as JMOD, is highly questionable and usually wrong (unless proven to give good results), the JMOD model was introduced not to get a good performance but for the sake of comparison among models. Because of the peculiar intramolecular conformation of EG molecules interacting through the JMOD force field, we consider worthwhile comparing the structural and dynamical properties with those of the other models. Furthermore, since the OPLS-like models (J, JMOD, and WP) have identical parameters for the intermolecular interactions, the comparison of the results obtained using these models will provide interesting insights into the understanding of the links between molecular shape and the intermolecular structure. In contrast to the previous WP and JMOD models that modify several aspects of the OPLS model, Hayashi and co-workers in Refs. 7 and 8 developed an entirely new force field for liquid EG. In this model, the long range interactions have a different set of parameters since effective charges were obtained from a fit of the intramolecular potential to *ab initio* calculations. Even the intramolecular potential is different from the OPLS-like ones since it introduces more minima in the purely torsional functions.

The intermolecular parts of the four potentials are pairwise additive functions which consist of simple Lennard-Jones plus Coulomb terms. In particular, the effective charges for the three different sites in the EG molecule were: $q_{\mathrm{H_O}}=0.435e$, $q_{\mathrm{O}}=-0.700e$, and $q_{\mathrm{Me}}=0.265e$ for the OPLS-like models, and $q_{\mathrm{H_O}}=0.523e$, $q_{\mathrm{O}}=-0.587e$, and $q_{\mathrm{Me}}=0.064e$ for the HTN model, where e is the electron charge. The Lennard-Jones parameters were identical for all the models.

The torsional motions about the Me−Me bond and the Me−O bonds were described by Fourier series for each dihedral angle with the particular functional form and parameters characteristic of each model. In Fig. 2, the Fourier series for all potential models and for the two different dihedral angles are plotted. In addition to the purely torsional terms, the intramolecular interactions were augmented by a Lennard-Jones term for the pairs of interaction sites within the same molecule separated by more than three (in the J and HTN models) or by more than two bonds (in the JMOD and WP models). In the case of the JMOD, WP, and HTN models, the nonbonded electrostatic interactions were also included for interaction sites separated by more than three bonds (JMOD and WP) or by more than two bonds (HTN), and the 2–5 interaction was also included in the HTN case.

C. Computational details

Molecular dynamics simulations of the four models for liquid ethylene glycol were performed at room temperature ($T=298$ K) and at the experimental density[43] at 1 atm on systems of 125 molecules which corresponds to a cubic box of side length $L=22.64$ Å.

The MD simulations have the same characteristics as those reported previously.[2] The classical equations of motion were integrated using the leap-frog Verlet algorithm[44] with a loose coupling to a thermal bath[45] and a time step of 2.5 fs. Results reported in this article were obtained after an MD run for each potential model consisting of an initial equilibration period of about 100 ps and the averages of the properties were computed over 900 ps.

Periodic boundary conditions were used in the simulations and constraints were handled by means of the SHAKE method.[46] The short-range forces were computed using a cutoff of half the size of the cubic cell length, $L/2$, and the long-range forces were taken into account by means of the Ewald summation technique.[47,48]

III. RESULTS AND DISCUSSION

A. Molecular conformation

The possibility of forming three-dimensional networks of hydrogen bonded molecules is linked with the conformational isomerism of the ethylene glycol molecule. Due to the restricted rotation about the central C–C bond, one *trans* and two *gauche* forms can exist. Each of these forms can be subdivided into several rotational isomers or rotamers according to the rotational state about the two C–O bonds. Theoretically, it is usually assumed that there are three minima in the potential for internal rotation about the three bonds. Thus, there are 27 ($=3^3$) theoretically possible rotational isomers. Some of these rotamers are related to one another by rotational symmetry. Therefore, there are only ten nonequivalent rotational isomers: six *gauche*, namely, $g^-G^-g^-$ (twofold degenerate), tG^-g^- (fourfold degenerate), $g^+G^-g^-$ (fourfold degenerate), tG^-t (twofold degenerate), g^+G^-t (fourfold degenerate), and $g^+G^-g^+$ (twofold degenerate); and four *trans*, namely, g^-Tg^- (twofold degenerate), tTg^- (fourfold degenerate), g^+Tg^- (twofold degenerate), and tTt; where *gauche* ($G^{\pm}$) and *trans* (T) conformers are termed with respect to the central C–C bond. Each conformer is identified in this way by the angles of its three backbone torsions. In some of the *gauche* rotamers, intramolecular hydrogen bonds may be formed while this possibility does not exist for the *trans* rotamers. One intramolecular hydrogen bond can be formed in $g^+G^-g^-$ and g^+G^-t rotamers and two intramolecular hydrogen bonds can be formed in the $g^+G^-g^+$ one. Intramolecular hydrogen bonds in this double cyclic ($g^+G^-g^+$) rotational isomer, however, must be very weak since they would be strongly stretched. In a liquid constituted by EG molecules with one intramolecular HB, one would expect linear chains of hydrogen bonding interacting molecules, whereas cyclic molecular aggregates may appear in systems with EG molecules with two intramolecular HBs. In the remaining situations, on the contrary, one expects three-dimensional networks of hydrogen bonded molecules.

As remarked previously, there is still some uncertainty about the equilibrium conformation of the ethylene glycol molecule, even though there is a great amount of experimental measurements and theoretical calculations on the gas phase. From electron diffraction measurements carried out on the free molecule, Bastiansen in Ref. 14 reported for the dihedral angle about the C–C bond, ϕ_{CC}, the value of 74°, which corresponds to a distance between the oxygen atoms in the molecule of $d(O\cdots O)\simeq 3$ Å. This distance is compatible with a *gauche* conformation with the possibility of internal hydrogen bonding. Yet, not all the *gauche* conformers can develop an intramolecular HB. From Bastiansen's experimental data, the *trans* rotamers seemed to be excluded.[49] Recent theoretical investigations using *ab initio* and semiempirical calculations of the isolated molecule[50] showed that *gauche* conformations with intramolecular HBs are the most favored energetically, in agreement with previous calculations.[51–57] The next most favored are the *trans* conformations and then the *gauche* conformations without intramolecular HBs. The specific energetic order of each of the ten independent rotational isomers depends slightly on the features of the basis set used in the calculations. From other theoretical studies on pure EG,[58] it was found that more than 30% of the molecules in the liquid have the two hydroxyl groups free to form HBs with the neighboring molecules, whereas this is true for at least 20% of the EG molecules in aqueous solution. In solvents of low dielectric constant, up to 20% of the EG was observed to be present as the *trans* isomer from nuclear magnetic resonance (NMR) measurements.[37] In the neat liquid this dropped to 14%.[59] From neutron diffraction experiments, by applying the isotopic substitution method together with simulation data obtained by means of the empirical potential Monte Carlo (EPMC) method,[60] Soper[38] reported a broad distribution of the central torsional angle with maxima at $\pm 69°$ and the existence of some degree of intramolecular hydrogen bonding.

In order to perform a quantitative analysis of the internal structure of the EG molecule, we have investigated the populations of the different isomers and the distribution of the dihedral angles ϕ_k associated with the torsional motions about the different bonds. To be able to carry out this study, the following definitions for the different conformers have been considered. The *trans* conformation is defined by the range $120° \leqslant \phi_k < 240°$ whereas the *gauche* conformations are defined by the ranges $0° \leqslant \phi_k < 120°$ (g^+) and $240° \leqslant \phi_k < 360°$ (g^-) for the OPLS-like models. In the case of the HTN model, we have adopted the definitions proposed in Ref. 8, which are given by the following ranges: $144° \leqslant \phi_k < 216°$, *trans*; $0° \leqslant \phi_k < 72°$ (g^+), and $288° \leqslant \phi_k < 360°$ (g^-), *gauche*; $72° \leqslant \phi_k < 144°$ (e^+) and $216° \leqslant \phi_k < 288°$ (e^-), *eclipsed*. In all cases, dihedral angles ϕ_k, which involve consecutive sites *A*, *B*, *C*, and *D*, are defined by the angle between the *ABC* plane and the *BCD* plane [see Fig. 1(b)]. For the three possible dihedral angles in the EG molecule, the situations displayed in Fig. 1(b) are the following:

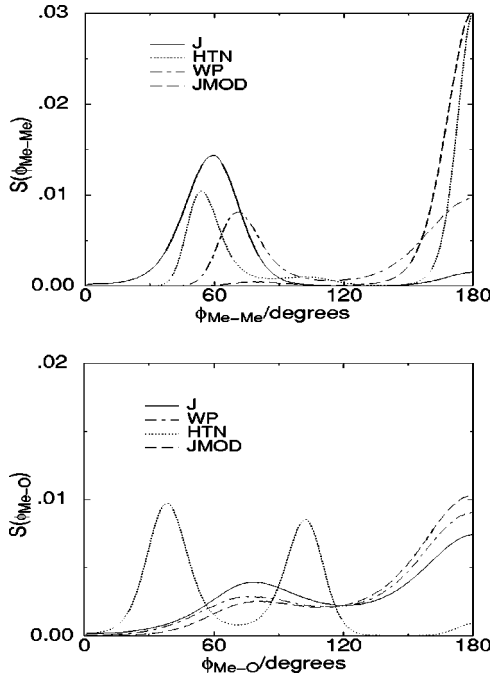

FIG. 3. Dihedral angle distribution for the torsional motions about the Me−Me (top) and Me−O (bottom) bonds. Due to symmetry, results for $S(\phi_{\mathrm{Me-O}})$ and $S(\phi_{\mathrm{O-Me}})$ have been averaged.

$\phi_{\mathrm{O-Me}}$ angle, $A=\mathrm{H_O}$, $B=$O, $C=$Me, and $D=$Me; $\phi_{\mathrm{Me-Me}}$ angle, $A=$O, $B=$Me, $C=$Me, and $D=$O; $\phi_{\mathrm{Me-O}}$ angle, $A=$Me, $B=$Me, $C=$O, and $D=\mathrm{H_O}$.

The molecular structure (molecular shape) has been studied through the analysis of several quantities. The distribution of dihedral angles, $S(\phi_k)$, for motions about the Me−Me and Me−O (or, equivalently, O−Me) bonds has been computed and is plotted in Fig. 3. The percentages of the different conformers are compared in Table I for the OPLS-like models and the results for the HTN model are summarized in Table II. An analysis of the distribution of the populations of each of the ten nonequivalent rotamers has also been performed and the results are compared in Tables I and III for the OPLS-like models. It is worth pointing out that there are more than ten nonequivalent rotamers for the HTN model due to the additional *eclipsed* form, which is not found in the other three models. In general, the intramolecular structure is quite different for all the models because of the different form of the intramolecular interactions.

The four models give fairly different results for the torsional motions about the central bond, Me−Me. All the $S(\phi_k)$ distributions for the OPLS-like models show a central peak and two mirror-image peaks (Fig. 3) corresponding to a *trans* and the two *gauche* conformations, respectively. In addition to these features, for the HTN model there are two extra peaks in the region corresponding to the *eclipsed* conformation for all the dihedral angles. These results were expected since each peak corresponds to the appropriate minimum in the torsional potential function (Fig. 2). The symmetry obtained for the calculated $S(\phi_k)$ distributions (data not shown) is evidence that the conformational equilibrium has been reached in all the simulations. In Fig. 3, the plotted results were obtained after averaging the curves about their symmetry axis.

TABLE II. Percentages of *gauche* and *eclipsed* conformers for the $\phi_{\mathrm{Me-Me}}$ and $\phi_{\mathrm{Me-O}}$ dihedral angles computed for the HTN model.

Model	*g* (Me–Me)	*e* (Me–Me)	*g* (Me–O)	*e* (Me–O)
HTN	32.5	9.3	55.5	43.2

Concerning the population of the different conformations of the $\phi_{\mathrm{Me-Me}}$ dihedral angle, the percentage of *gauche* conformers (45.2%) is slightly lower than the percentage of *trans* conformers for the WP model. In the case of the J model, most of the molecules adopt a *gauche* conformation and only about 5% of the molecules remain in a *trans* state. Conversely, in the JMOD model, the majority of molecules have a *trans* conformation and the percentage of *gauche* conformers is less than 5%. For the HTN model, the percentage of *trans* conformers (58%) is similar to that found for the WP model. The percentage of *gauche* conformers is greater than that of *eclipsed* conformers and lower than that of *trans* conformers for this (HTN) model. With regard to the populations of the $\phi_{\mathrm{Me-O}}$ dihedral angles, the percentages of *trans* conformers (ranging from 51.8% for J to 68.4% for JMOD) are greater than those observed for the *gauche* conformers for all the OPLS-like models. The largest differences between *gauche* and *trans* populations are observed in the JMOD model, whereas the J model show quite similar populations for both states. In the case of the HTN model, the percentage of *gauche* conformers is greater than that of *eclipsed* conformers and the percentage of *trans* conformers is less than 2%.

As observed previously for the populations of the different conformations, the position of the maxima of the $S(\phi_k)$ functions and their widths are dependent on the potential model considered, especially in the case of the $\phi_{\mathrm{Me-Me}}$ dihedral angle. The *gauche* maxima are located at about $\pm 60°$ for the J model whereas they are shifted to larger angles (in absolute value) for the WP model ($\sim \pm 75°$) and to even greater angles for the JMOD model ($\sim \pm 80°$). The positions of the maxima corresponding to the *gauche* conformation correspond to smaller angles for the HTN model ($\sim \pm 50°$)

TABLE I. Population of the different isomers and percentages of conformers for Me−Me and Me−O dihedral angles for the OPLS-like models. *Gauche* conformation.

Model	$g^-G^-g^-$	tG^-g^-	$g^+G^-g^-$	tG^-t	g^+G^-t	$g^+G^-g^+$	Me−Me	Me−O
J	9.7	47.6	7.4	27.0	0.2	3.7	94.8	48.2
JMOD	<0.1	0.3	0.2	0.9	1.7	0.3	3.4	31.6
WP	0.5	4.0	3.4	10.6	21.7	4.8	45.2	37.1

TABLE III. Population of the different isomers for the OPLS-like potential models. *Trans* conformation.

Model	g^-Tg^-	tTg^-	g^+Tg^-	tTt
J	2.5	1.8	<0.1	<0.1
JMOD	4.1	41.9	5.1	45.5
WP	2.1	21.0	2.8	28.9

than those found for the J model. On the contrary, the peak corresponding to the *trans* conformation is always located at 180° due to symmetry. The widths of the maxima are considerably different for all the models. The *gauche* maxima are wider for the J and JMOD models (~30°) than for the WP and HTN models (~20°). This situation change for the *trans* maximum. For this conformation, the widest maximum is observed for the WP (~50°) model while we obtained similar widths for the J and JMOD models (~30°) and the narrowest maximum was found for the HTN model (~15°). The distributions of the $\phi_{\mathrm{Me-O}}$ dihedral angles are quite broad for all the force fields and the maxima are located at similar positions for the OPLS-like models. In the case of the HTN model, the distributions are narrower. The existence of nonzero minima between the diverse maxima for both dihedrals indicates the presence of transitions among the different conformations. It is interesting to note that, for instance, for the $\phi_{\mathrm{Me-Me}}$ dihedral angle, the curve in the case of the WP model presents more transitions than in any other model, which indicates a more pronounced flexibility.[61]

The populations of the different rotamers are reported in Tables I and III for the OPLS-like force fields. The most unfolded conformations are preferred by the JMOD and WP models (tTt and tTg^-) whereas the most folded geometries are more probably displayed by the WP (g^+G^-t) and J ($g^+G^-g^-$) models. In particular, for the J model, the most probable conformations are the following: tG^-g^-, with a population corresponding to about half of the molecules, and $g^+G^-g^-$. Moreover, 11.3% of molecules have a conformation where one (7.6%) or two intramolecular HBs might be found. For molecules interacting via the JMOD potential, however, the most populated states are tTt and tTg^-, where intramolecular hydrogen bonding is not possible. For the WP model, however, the isomers with significant populations are tTt, tTg^-, and g^+G^-t. In the latter model, about 30% of the molecules have a conformation where one (25.1%) or two intramolecular HBs might be found. The comparison between JMOD and WP models (Table I) indicates an increase (preference) of the *gauche* conformation population about the Me–O bonds when the Me–Me dihedrals adopt a *gauche* conformation. This preference is consistent with favorable intramolecular interactions and the possible formation of intramolecular HBs in $G^{\pm}g^{\mp}$ (or $g^{\pm}G^{\mp}$) conformations, which is impossible in $G^{\pm}t$ (or $tG^{\mp}$) conformations. Actually, this increase in the population of *gauche* Me–O conformations when the Me–Me conformation is *gauche* leads to a considerable increase in the population of the g^+G^-t rotamer (which has the possibility of formation of one intramolecular HB) for the WP model (21.7%) compared to the JMOD model (1.7%).

In conclusion, J, WP, and HTN models agree reasonably well with the experimental data, although the HTN model differs from the usual conformational considerations. The *gauche* maxima of the J and HTN models are located at angles somewhat smaller than those expected from the available experimental data, i.e., ±74° for the gas phase as obtained by electron diffraction measurements;[14] whereas the WP model gives results very close to experiments. Nevertheless, the values obtained for the J model agree with those reported from empirical simulations[38] of liquid EG (±65°). These empirical calculations, however, show quite broad maxima. The J and WP models, in addition, give reasonable values for the populations of those *gauche* conformations about the Me–Me bond with the possibility of intramolecular HBs, which were predicted to be the most favorable energetically from theoretical calculations. Finally, even though the JMOD model gives completely unreasonable results for the molecular conformation of the EG molecule, as expected, its distinctive intramolecular structure will be very useful for the sake of further comparison between the models, especially to address issues such as the molecular shape influence upon the intermolecular structure of the liquid.

B. Intermolecular radial distribution functions

Radial distribution functions (RDFs) provide an important description of the structure in a liquid. In the case of ethylene glycol, due to symmetry and to the consideration of only three different sites in the molecule (two hydroxyl hydrogen atoms, two oxygen atoms, and two methylene groups), only six nonequivalent site–site radial distribution functions, namely, $g_{\mathrm{HH}}(r)$, $g_{\mathrm{OO}}(r)$, $g_{\mathrm{MeMe}}(r)$, $g_{\mathrm{OH}}(r)$, $g_{\mathrm{OMe}}(r)$, and $g_{\mathrm{HMe}}(r)$, exist. The six site–site RDFs have been computed for all the potential models studied and four of them, specifically, $g_{\mathrm{OO}}(r)$, $g_{\mathrm{OH}}(r)$, $g_{\mathrm{MeMe}}(r)$, and $g_{\mathrm{MeH}}(r)$, are plotted in Fig. 4. The $g_{\mathrm{HH}}(r)$ function is shown at the top of Fig. 5. Notice that in hydrogen bonded liquids the most structured and interesting RDFs are those involving the oxygen and hydrogen atoms of the hydroxyl groups. We observed an overall agreement of the results obtained for the RDFs of the four simulated systems. This is the case even for the HTN potential for which a different set of effective charges was used. For those RDFs involving hydrogen and oxygen atoms, the largest deviations from the general characteristics are observed for the J model. As a general trend, these $g_{\alpha\beta}(r)$ for the J model show lower maxima and less deep minima located at the same positions as those for the other OPLS-like models and even those for the HTN model [except for the $g_{\mathrm{HH}}(r)$ function whose first maximum is shifted to larger distances for the HTN model]. The main discrepancies among the models are observed only beyond the first peak. The higher values for the $g_{\alpha\beta}(r)$ for O–O and O–H at the first minima indicate that the first coordination shell is less well-defined for the J model than for the others. The effect of the intramolecular conformation on the intermolecular structure is particularly evident in this case. The fact that most of the molecules interacting through the J potential adopt a *gauche* conformation affects the hydrogen bonding structure by weakening the HBs. The *gauche* conformation constrains the O–O intramolecular distances to

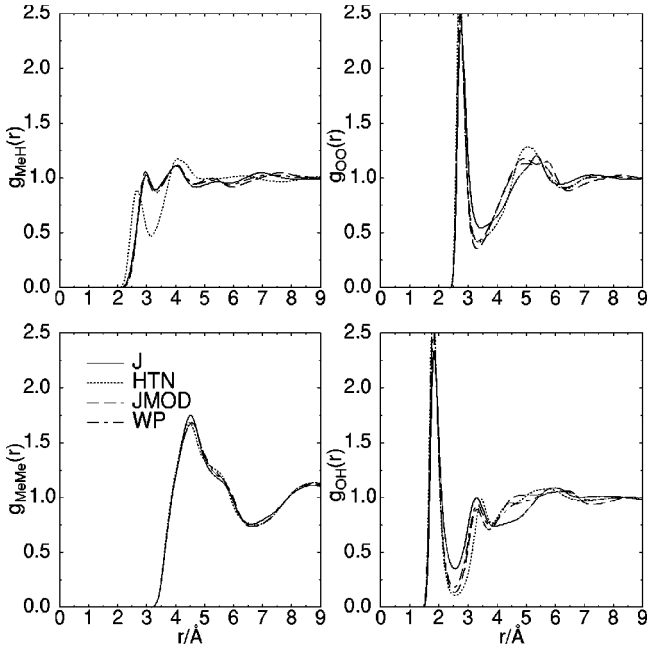

FIG. 4. From left to right: partial site–site radial distribution functions for MeH and OO (top); partial site–site radial distribution functions for MeMe and OH (bottom). Simulated curves for the four potentials are given. Symbols are J (solid line), JMOD (long dashed line), WP (dot-dashed line), and HTN (dotted line).

their closest values so it is more difficult to accommodate the two expected intermolecular HBs per hydroxyl group due to steric hindrance. In the models with mostly *trans* or mixed conformations, the hydroxyl groups are more free and can more easily rearrange and promote more favorable hydrogen bonding interactions with less steric encumbrance. Conversely, when those $g_{\alpha\beta}(r)$ involving the Me atoms and either H or O are examined, the greatest discrepancies are found for the HTN model. This is due to the almost null charge located at the Me position in HTN. It is remarkable, however, that we find no difference among the models for $g_{\mathrm{MeMe}}(r)$. In fact, the $g_{\mathrm{MeMe}}(r)$ obtained for EG is rather similar to the $g_{\mathrm{Me_OMe_O}}(r)$ we previously obtained for liquid ethanol ($\mathrm{Me_C-Me_O-O-H_O}$) with the OPLS potentials (see Ref. 3, Fig. 4). This suggests a similar packing of Me–Me groups in liquid EG at room temperature and $\mathrm{Me_OMe_O}$ groups in ethanol, mainly governed by the short-range interactions evidenced by the absence of any effect in the $g(r)$ upon changing the effective charges on the Me sites or upon variation of the molecular shape. Note, however, the strong influence of the different set of charges on the $g_{\mathrm{MeH}}(r)$ (Fig. 4) and $g_{\mathrm{MeO}}(r)$ (data not shown), whereas the differences in molecular shape have only a very minor effect.

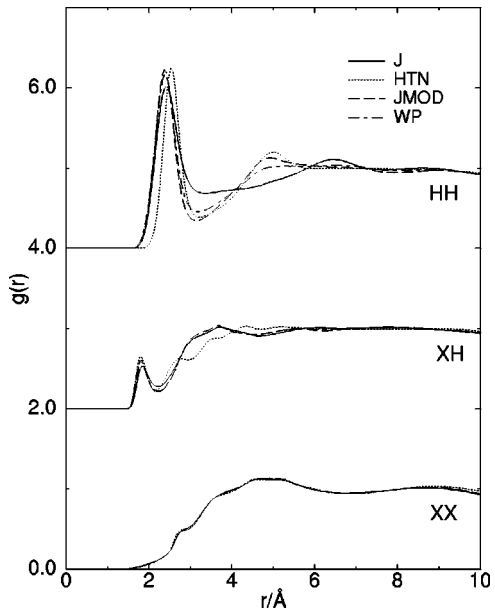

FIG. 5. Simulated $g_{\mathrm{XX}}^{(\mathrm{inter})}(r)$, $g_{\mathrm{XH}}^{(\mathrm{inter})}(r)$, and $g_{\mathrm{HH}}^{(\mathrm{inter})}(r)$ functions, as described in the text, for the four potentials. $g_{\mathrm{XH}}^{(\mathrm{inter})}(r)$ and $g_{\mathrm{HH}}^{(\mathrm{inter})}(r)$ curves are shifted vertically with regard to $g_{\mathrm{XX}}^{(\mathrm{inter})}(r)$ by a constant of 1.0 and 2.0, respectively.

We have studied the radial distribution functions of the molecular centers-of-mass and the molecular orientations in the liquid. The orientational correlations in molecular liquids can be analyzed through the functions[62]

$$Gl(r)=\langle P_l[\cos\vartheta(r)]\rangle, \tag{1}$$

where P_l is the lth Legendre polynomial and $\vartheta(r)$ is the angle between the dipole moments of two molecules whose centers-of-mass are located at a distance r. We have calculated Gl for $l=1$ and 2 and the results obtained are shown in Fig. 6. The radial distribution function of the molecular centers-of-mass is also shown in Fig. 6 for the four models. In general, the computed Gl functions show a fast decay of the orientational correlations when the distance between molecular centers-of-mass increases. Thus, we have found that for distances greater that the maximum of the $g(r)$ for the molecular centers-of-mass (see Fig. 6, bottom) the correlations fade out, whereas for smaller distances [see plot for $G1(r)$] the tendency of neighboring molecules is to orient their dipole moments in the same direction, indicated by the positive values of $G1$. This parallel orientation of the molecular dipoles for neighboring molecules is also found in water and short alkanols.[1,3] In the case of WP, however, molecules whose centers-of-mass are separated by 3–4 Å have molecular dipoles pointing in opposite directions (shown by the negative $G1$ values). Concerning the radial distribution function of the molecular centers-of-mass, its main feature for all the potentials is the broad first maximum at about 4.9 Å and the first minimum at 6.7 Å. Differences appear for the J model for which a small maximum at about 3.4 Å is present and the first peak, which now is lower than that of the JMOD, WP, and HTN models, is split into two. This evidences again the effect of molecular conformation on the intermolecular structure. Specifically, the similarities between models with mostly *trans* conformations and with mixed *trans*/*gauche* conformations and the discrepancies between this group and models with mostly *gauche* conformers is, in this case, observed in the RDFs of the molecular centers-of-mass.

C. Comparison of MD results with neutron diffraction data

Several neutron diffraction experiments on liquid EG can be found in the literature[38,39] whereas, to our knowledge,

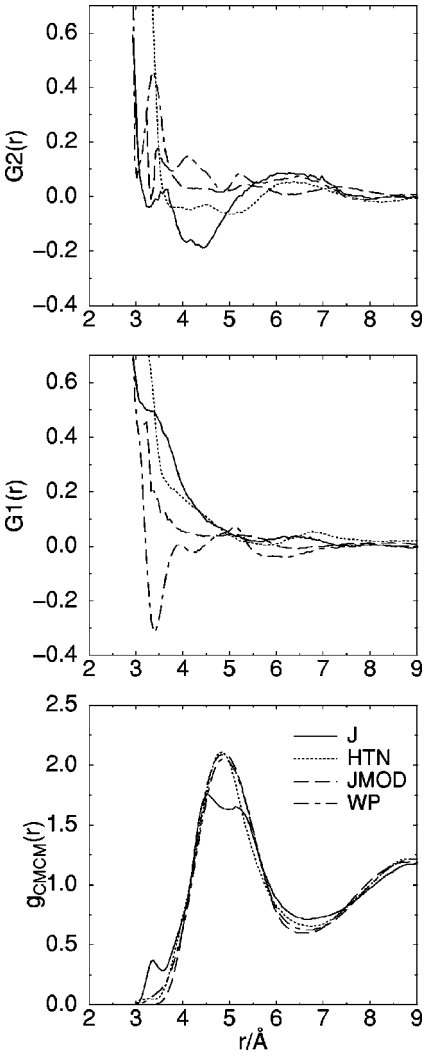

FIG. 6. Radial distribution function of the molecular center-of-mass and orientational correlation functions $[Gl(r),\ l=1,2]$ for the four studied models. Symbols are the same as in Fig. 4.

there is no x-ray scattering data available. Salmon and coworkers studied ionic solutions in hydrogen bonded solvents, in particular ethylene glycol and glycerol.[40] In the case of EG, the total structure factor of a fully deuterated sample ($D-O-CD_2-CD_2-O-D$) was also obtained by the authors.[39] The method of H/D isotopic substitution was used by Soper[38] to obtain several radial distribution functions after performing experiments on three different samples of EG: (1) a fully deuterated sample ($D-O-CD_2-CD_2-O-D$), (2) a sample with protonated hydroxyl hydrogens and with hydrogens in the methyl groups fully deuterated ($H-O-CD_2-CD_2-O-H$), and (3) an equimolar mixture of (1) and (2). In this method, by analyzing separately solutions with the same stoichiometry but with different isotopic compositions, it is possible to identify the different correlations involving the isotopically substituted sites from the complex diffraction pattern. In our case, the hydrogen atoms (H) in the EG molecule are substituted by deuterium atoms (D) at different positions. Following this procedure, three independent distribution functions were obtained from the three samples, namely, $g_{\mathrm{HH}}(r)$, $g_{\mathrm{XH}}(r)$, and $g_{\mathrm{XX}}(r)$,[38] where H corresponds to the hydrogen atoms of the hydroxyl groups and X corresponds to all the atoms in the EG molecule except the hydrogen atoms of the hydroxyl groups.

In order to compare our results with the latter experimental data we have obtained the radial distribution functions $g_{\mathrm{HH}}(r)$, $g_{\mathrm{XH}}(r)$, and $g_{\mathrm{XX}}(r)$ in terms of the partial site–site radial distribution functions, $g_{\alpha\beta}(r)$, computed during the simulations. Notice that the structure factors obtained experimentally contain correlations among atoms in different molecules (intermolecular) as well as within the same molecule (intramolecular). In Fig. 5, the results obtained from the simulations for the $g_{\mathrm{HH}}^{(\mathrm{inter})}(r)$, $g_{\mathrm{XH}}^{(\mathrm{inter})}(r)$, and $g_{\mathrm{XX}}^{(\mathrm{inter})}(r)$ distribution functions, which involve only intermolecular correlations, are plotted. Explicitly, these functions are given by

$$g_{\mathrm{XH}}^{(\mathrm{inter})}(r)=1+\frac{1}{c_X b_X}\sum_{\beta\in X} c_\beta b_\beta (g_{H\beta}^{(\mathrm{inter})}(r)-1), \tag{2}$$

and

$$g_{\mathrm{XX}}^{(\mathrm{inter})}(r)=1+\frac{1}{c_X^2 b_X^2}\sum_{\alpha,\beta\in X} c_\alpha c_\beta b_\alpha b_\beta (g_{\alpha\beta}^{(\mathrm{inter})}(r)-1), \tag{3}$$

where all the $g_{\alpha\beta}^{(\mathrm{inter})}(r)$ and $g_{HH}^{(\mathrm{inter})}(r)$ are the intermolecular partial site–site RDFs computed during the MD simulations, which were discussed in the previous section. The c_X and b_X quantities are defined by

$$c_X=\sum_{\alpha\neq H} c_\alpha \quad \text{and} \quad b_X=\sum_{\alpha\neq H} c_\alpha b_\alpha / c_X, \tag{4}$$

respectively. Here, c_α is the atomic fraction of species α and b_α is the neutron scattering length of species α. Note that the $g_{\mathrm{HH}}(r)$, $g_{\mathrm{XH}}(r)$, and $g_{\mathrm{XX}}(r)$ functions reported in Ref. 38 are simply the inverse Fourier transform of the structure functions $H_{\mathrm{HH}}(Q)$, $H_{\mathrm{XH}}(Q)$, and $H_{\mathrm{XX}}(Q)$, respectively, which are actually the quantities measured experimentally. Although the molecular model we have used does not consider the hydrogen atoms of the methylene groups (henceforth termed, M) explicitly and, hence, no interaction sites were placed in the position of these atoms, we have included the four atoms in a geometrical way in order to compute the correlations involving the M atoms. The inclusion of the correlations involving these atoms is crucial because these are the most dominant contributions when one deals with neutron scattering experiments. The imposed geometrical constraints for the M atoms are the following: (1) the distance between the carbon atom (Me) and the hydrogen M atom is $d(\mathrm{C-M})=1.0936$ Å, (2) the angle defined by the Me–Me–M atoms is $\angle \mathrm{CCM}=110.297°$, and (3) the angle between the O–Me–Me plane and M–Me–Me plane is $\overbrace{\mathrm{OCC}}\ \underbrace{\mathrm{MCC}}=120.0°$. The latter condition leads to a value of 108.633° for the $\angle$MCM angle.

In the case of the $g_{\mathrm{XX}}^{(\mathrm{inter})}(r)$function (Fig. 5, bottom), the four models give practically the same result. To compare our results with the experiments (see Ref. 38), it should be noted that these neutron scattering data also include the intramolecular correlations whose main contributions are those due

to the nearest-neighbor (n) and next-nearest-neighbor (nn) atoms within the molecule (peaks located at, n: $r_{MC}=1.0$ Å, $r_{OC}=1.4$ Å, $r_{CC}=1.5$ Å, $r_{MM}=1.7$ Å, and $r_{MO}=2.0$ Å; and nn: $r_{MC}=2.1$ Å and $r_{OC}=2.4$ Å).[63] For the $g_{XH}^{(inter)}(r)$ curves, all the OPLS-like potential models give similar results whereas the HTN model is somewhat different at intermediate distances. This is due to the discrepancies found in the $g_{MeH}(r)$ function (Fig. 4) in the previous section. However, as in the case of the $g_{XX}(r)$ functions, there is an overlap between intramolecular and intermolecular correlations from 2 to 4.4 Å and the peaks due to nearest-neighbor and next-nearest-neighbor atoms within the molecule will be located[63] at 0.945 Å (r_{OH}) and 1.9 Å (r_{CH}). The good agreement found is an indication that the overall structure is well-reproduced by the studied force fields. Since marked differences are not observed among the different models, however, these experimental data alone are unable to select the most realistic one.

The $g_{HH}^{(inter)}(r)$ function (see Fig. 5, top) presents the most important discrepancies between the models. For the OPLS-like models, the first peak is located at very close positions ($r=2.4$ Å, for JMOD and WP, and $r=2.45$ Å, for J). For the HTN model, however, the first peak is slightly shifted ($r=2.55$ Å) because the effective charge on the H_O site is larger for this model. The results for the first peak are in good agreement with the experimental data[38] where the $g_{HH}(r)$ function displays a maximum at 2.4 Å, though lower in height than that of the simulations. Therefore, the peak found experimentally may be associated with intermolecular hydrogen bonding rather than with intramolecular correlations. The height of the first peak for the HTN model is very similar to that for the JMOD and WP models, which is consistent with the similar results also obtained for the O−O and O−H distributions. The height of the first peak for the J model, however, is slightly lower. The first minima is located at 3.2 Å for all the models but it is deeper for the JMOD, WP, and HTN models than for the J model, which, as indicated in the previous section, agrees with the not-so-well-defined distances for the HBs in the J case. A small second maximum was found for the HTN and JMOD force fields at 5 Å and for the J model at 6.5 Å, whereas for the WP force field $g_{HH}(r)$ is structureless for $r>5$ Å. Intramolecular and intermolecular overlapping contributions are observed in the 1.3−5.1 Å region for the simulated $g_{HH}(r)$. No evidence of a peak has been found, however, at this distance for any of the analyzed potentials. It is interesting to note that experimental data show a shoulder in the HH distribution function between 1.5 and 2 Å. In the case of the HH correlations, we have also computed the radial distribution functions for hydrogen atoms of the hydroxyl group located within the molecule, i.e., $g_{HH}^{(intra)}(r)$, in order to investigate whether this shoulder can be associated to intramolecular distances or not. In this region, a broad maximum has been observed for the J model (data not shown). In the rest of the models, this function is zero up to distances of ≈ 2 Å for the most favorable situation, which corresponds to the HTN and WP models. Therefore, only the J model qualitatively reproduces this particular feature of the experimental $g_{HH}(r)$ in this region.

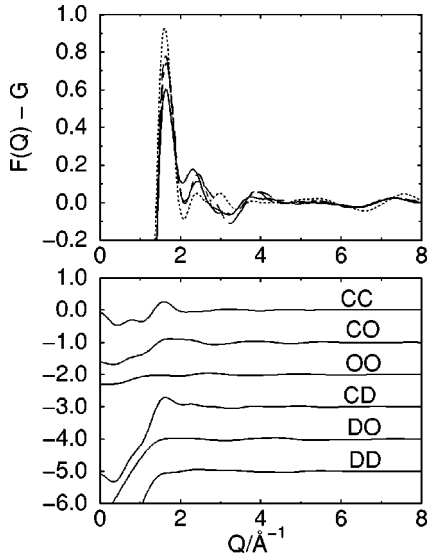

FIG. 7. $[F(Q)-G]$ function (top). Calculated data from the simulations: J (full line), JMOD (long dashed line), WP (dot-dashed line), and HTN (dotted line). Intermolecular contributions to the $[F(Q)-G]$ function for the J model (bottom). For the sake of clarity, curves have been shifted vertically by multiples of −1.0.

The direct comparison between the experimental data from Ref. 38 and the present simulation results suggests that more realistic molecular models including other intramolecular motions such as stretching and (chiefly) bending modes should be considered in order to be able to obtain a better agreement. We have found, however, a global accord between the obtained results for all the models and the experimental data.

In order to compare the simulation results with those from Ref. 39, the appropriate expressions in terms of the computed quantities have to be used. Thus, for the fully deuterated sample,[39] the structure factor can be written as

$$F(Q)-G=\sum_{\alpha}\sum_{\beta} c_{\alpha}c_{\beta}b_{\alpha}b_{\beta}(S_{\alpha\beta}(Q)-1), \tag{5}$$

with $\alpha,\beta=C,D,O$, and $S_{\alpha\beta}(Q)$ given by

$$S_{\alpha\beta}(Q)-1=4\pi\rho\int_0^{\infty} r^2[g_{\alpha\beta}(r)-1]\frac{\sin Qr}{Qr}dr, \tag{6}$$

where $S_{\alpha\beta}(Q)-1=H_{\alpha\beta}(Q)$, and

$$G=\sum_{\alpha} c_{\alpha}(b_{\alpha}^2+b_{\alpha,\mathrm{inc}}^2), \tag{7}$$

$b_{\alpha,\mathrm{inc}}$ being the incoherent neutron scattering length. In the previous equations, ρ is the total atomic number density of the system. Note that the b_{α} now become b_D for all the hydrogen atoms in the molecule.

The main feature of the results obtained for the $F(Q)$ curves for the four models is the first peak at 1.6 Å^{-1} (Fig. 7, top). This is in excellent agreement with the experimental value of 1.5 Å^{-1} (Ref. 39). Since MD simulations allow us to extract the different components of the contributions to the total structure factor obtained experimentally, we display in Fig. 7 (bottom) the different contributions, with their weight-

TABLE IV. Percentages of molecules with n hydrogen bonds (where $n=0,1,2,3,4\ldots$) and mean number of hydrogen bonds per molecule $\langle n_{HB}\rangle$ for the four potential models.

	n							
Model	0	1	2	3	4	5	$\geqslant 6$	$\langle n_{HB}\rangle$
J	<1	<1	4	25	53	16	1	3.8
JMOD	<1	<1	5	27	58	9	<1	3.7
WP	<1	1	6	29	54	10	<1	3.7
HTN	<1	<1	6	23	68	2	<1	3.6

TABLE V. Percentage of OH groups with n hydrogen bonds and mean number of hydrogen bonds per OH group $\langle n_{HB}^{OH}\rangle$ for all the simulated potential models. Values in parenthesis correspond to the percentage of oxygen atoms which participate in n hydrogen bonds as proton acceptor.

	n					
Model	0	1	2	3	$\geqslant 4$	$\langle n_{HB}^{OH}\rangle$
J	1 (16)	19 (71)	65 (13)	14 (<1)	<1 (<1)	1.9
JMOD	1 (12)	18 (82)	75 (6)	6 (<1)	<1 (<1)	1.9
WP	1 (16)	20 (75)	71 (8)	7 (<1)	<1 (<1)	1.8
HTN	1 (15)	17 (81)	80 (4)	1 (<1)	<1 (<1)	1.8

ing factors included, to the function $F(Q)-G$ for the J model case. From the simulations, it is observed that the most important contributions to this maximum are those arising from CC and CD. Yet, CO and DO also contribute in this region, though to a lower degree. Since in the plotted data we have only included the intermolecular distribution functions, even though the experimental curves contain intramolecular as well as intermolecular contributions, the origin of the first maximum is mainly due to intermolecular correlations whereas the features found for values of Q greater than 4 $Å^{-1}$ (in this region the experimental curve displays oscillations)[39] are due to intramolecular correlations. Experimental data and simulation results are again found to be in an overall agreement. As in the experiment described before, however, these data cannot be used alone to discriminate between the models. To summarize, we have found a good qualitative agreement between structural experimental data and simulation results, which spans from small distances (experiments in Ref. 38 and simulations) to longer distances (experiments in Ref. 39 and simulations), for all the studied models.

D. Hydrogen bonding statistics

The intermolecular hydrogen bonding statistics have been analyzed for the four potential models. A geometric criteria similar to that considered in our previous work[2] was used for the definition of a hydrogen bond for liquid ethylene glycol. Thus, we assumed that an intermolecular HB between two molecules ($O^{\sharp}-H\cdots O^{*}$) exists if the following three conditions are fulfilled. First, the distance between the oxygen atoms is smaller than R_{OO}^{C}. Second, the distance between the oxygen atom ($O^{\sharp}$) of one molecule, which acts as proton donor in the hydrogen bond, and the hydrogen atom of the other molecule, covalently bonded to the oxygen atom (O^{*}), which acts as proton acceptor in the HB, is smaller than R_{OH}^{C}. Third, the $H-O^{\sharp}\cdots O^{*}$ angle is smaller than φ^{C}. The distances R_{OO}^{C} and R_{OH}^{C} are usually chosen as the positions of the first minima of the radial distribution functions $g_{OO}(r)$ and $g_{OH}(r)$ (see Fig. 4), respectively. We chose the same R_{OO}^{C} and R_{OH}^{C} values as those used previously for methanol and ethanol[2–4] for the OPLS-like models because the minima of the RDFs are located at similar positions. In the case of the HTN model, we adopted a slightly smaller value for R_{OO}^{C}, specifically, $R_{OO}^{C}=3.38$ Å. In all cases, we used the same value for φ^{C} ($\varphi^{C}=30°$).

The percentages of molecules with n hydrogen bonds ($n=0,1,2,3,4\ldots$) and the mean number of hydrogen bonds per molecule, $\langle n_{HB}\rangle$, are reported in Table IV for all the studied models. In Table V, the percentages of hydroxyl groups with n hydrogen bonds ($n=0,1,2,3,4\ldots$) and the mean number of hydrogen bonds per hydroxyl group, $\langle n_{HB}^{OH}\rangle$, are compared. We summarize the percentages of oxygen atoms participating in n hydrogen bonds as proton acceptors in Table V, as well. We obtained similar results for all the models. In general terms, the mean number of HBs per molecule is slightly lower than four. This suggests the presence of three-dimensional patterns of hydrogen bonded molecules in the liquid, regardless of the mean conformation of the molecule. Furthermore, most of the molecules participate in four intermolecular HBs, about 25% of them participate in three HBs, and there is also a considerable amount of molecules with five HBs. Notice that a small fraction of molecules, which is essentially the same for all the studied models, participate in two HBs. Concerning hydrogen bonding of the hydroxyl groups (Table V), the mean number of HBs per hydroxyl group and the computed values for the populations of the $n=0,1$ states is similar for all the models, despite the differences observed in the populations of $n=2,3$ states.

There is a rather small fraction (3%) of ''multiple'' hydrogen bonds, i.e., hydrogens directly hydrogen bonded to more than one oxygen atom or oxygen atoms participating as proton acceptors in more than two hydrogen bonds, for the J model. Specifically, for this model multiple intermolecular HBs arise from hydrogen atoms simultaneously hydrogen bonded to more than one oxygen atom (Table V).

We did not observe significant differences when the values of R_{OO}^{C} or R_{OH}^{C} or both were slightly changed. Although variations of the φ^{C} parameter ($\varphi^{C}>30°$) lead to differences in the percentages obtained, especially for the J model (with broader distributions of the φ angles), these differences are minor and so the intermolecular hydrogen bonding picture of the fluid is not seen changed.

E. Self-diffusion coefficients

The self-diffusion coefficients, D, for the four potentials have been determined from the slope of the mean-square displacement of the molecular centers-of-mass through the Einstein formula

$$D=\lim_{t\to\infty}\frac{\langle (R_i(t)-R_i(0))^2\rangle}{6t}. \tag{8}$$

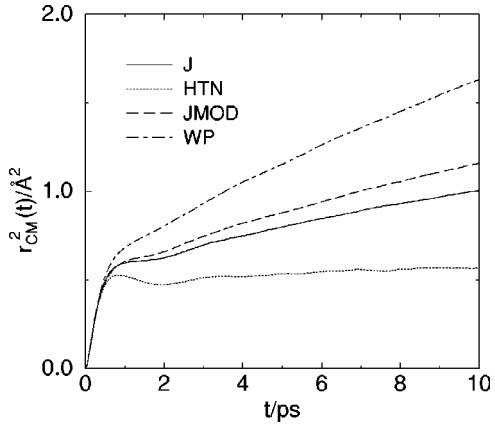

FIG. 8. Mean-square displacements of the molecular centers-of-mass for the four models.

In Fig. 8, we compare the curves obtained for the mean-square displacement of the molecular centers-of-mass for the different models. We obtained the following values: $D = 7.4\times10^{-7}$ cm^2s^{-1} (J), 11.7×10^{-7} cm^2s^{-1} (JMOD), 17.0×10^{-7} cm^2s^{-1} (WP), and 2.5×10^{-7} cm^2s^{-1} (HTN). The self-diffusion coefficients show marked discrepancies for the different potentials. Discrepancies of almost an order-of-magnitude are found for the highest and the lowest self-diffusion coefficients. In the case of the OPLS-like models, for which the intermolecular parameters are identical, there is a factor of 2.3 between the highest and the lowest *D*. The fastest dynamics is displayed by the WP model whereas the slowest one is obtained for the HTN model. Concerning the intermediate dynamics, the JMOD model diffuses faster than the J one. Recently, an experimental value of 9.0×10^{-7} cm^2s^{-1} for *D* has been reported for ethylene glycol at room temperature.[64] Therefore, the results obtained for the OPLS-like models, especially for the J and JMOD models, are in reasonable agreement with the experiments whereas the *D* value for the HTN model is too low.

It is worth noting that, although hydrogen bonds strongly influence the molecular diffusion in hydrogen-bonded liquids,[4] the discrepancies observed in the self-diffusion coefficients for the studied models cannot arise from differences in the intermolecular network of HBs since we have found a similar picture for all of them, as discussed in the previous section. The mean molecular shape also seems to have only minor effects and quite similar results are found for fluids with most of their molecules in a *trans* state (JMOD model) and for systems with most of their molecules adopting a *gauche* geometry (J model). The model with the fastest diffusion, however, also presents frequent transitions[61] from one conformation to the other. Thus, our results indicate a coupling between intramolecular motions and self-diffusion. These findings are consistent with results described in Ref. 65 for liquid *n*-alkanes where a coupling between the intramolecular dynamics and the intermolecular one was also found to be rather important. For those systems, it was reported a 70% enhancement of the self-diffusion coefficient when a six-interaction-site molecule with fixed bond lengths and bond angles but without any constraint for the torsional motions $[V(\phi)=0]$ was compared with a model liquid hexane with fixed bond lengths and bond angles but nonnull torsional potential $[V(\phi)\neq0]$. In that case, the diffusion of the more flexible molecule was faster than that of the model hexane.

IV. CONCLUDING REMARKS

We have examined the structure of liquid ethylene glycol at room temperature by performing a molecular dynamics simulation study with several force fields. A thorough analysis of the molecular conformation of ethylene glycol has been carried out for the different potentials in order to understand which factors may lead to differences in the computed properties. Our work suggests that one of the studied models, namely, J is a suitable candidate for the study of the real liquid. The WP model, however, gives reasonable results for both the molecular conformation and the intermolecular structure, while the self-diffusion coefficient is twice as large as the experimental value.

Concerning the intramolecular structure, the J and WP models give a molecular conformation in accordance with the available experimental data and theoretical calculations, where the molecule was found more likely to adopt a *gauche* conformation. In these two models, we found that the EG molecule takes the most extended conformations in the WP model and the most folded structure in both the J and WP models. Furthermore, for these models the populations of conformations where intramolecular hydrogen bonds may be present (about 30% and 11% for the WP and J models, respectively) were in good agreement with experiment and theoretical calculations. Although the HTN model differs from the usual conformation considerations, the results obtained for the molecular conformation are in reasonable agreement with experiment.

The four analyzed potential models of liquid ethylene glycol give a similar picture for the intermolecular structure and we observed a general (qualitative) agreement with neutron scattering experiments. We found that the structure is dominated by three-dimensional networks of hydrogen bonded molecules with a mean number of hydrogen bonds per molecule slightly lower than four. These two characteristics are similar to those of liquid water. However, it should be noted that the singular tetrahedral geometry of the hydrogen bonding patterns in water cannot be achieved by EG due to its molecular geometry and the presence of the methylene groups. In agreement with results found for water and short alkanols, neighboring EG molecules have the tendency to orient their molecular dipoles parallel regardless of the model considered. Surprisingly, these characteristics hold, irrespective of the model used and we obtained similar results for each model, which were independent of the mean conformation of the molecule. Models which would allow a relatively high degree of intramolecular hydrogen bonding and models, such as JMOD, which basically adopt a *trans* conformation where no intramolecular hydrogen bonding is possible gave similar results. This indicates that from the intermolecular structural data alone one cannot infer whether or not there is competition between intramolecular and intermolecular hydrogen bonds. Therefore, it seems that the presence or absence of intramolecular hydrogen bonds does not

apparently affect the general intermolecular picture of the condensed phase. The molecular shape, however, has been observed to have some effect on the intermolecular structure. In the model system with most of the molecules in the *gauche* conformation (J model), for instance, the constraint of the intramolecular oxygen–oxygen distances to their closest values by the *gauche* state affects the intermolecular structure by weakening the HBs, so they display geometries not as well defined as in the rest of the models which have mixed *trans/gauche* conformations or mostly *trans* conformations.

The results obtained for the dynamics indicate that the distinct models give quite different results for the dynamical properties despite the similarities found in the intermolecular structure. Hence, the comparison with experimental dynamical quantities for liquid ethylene glycol seems crucial in discriminating amongst the different models in order to select the most realistic one. Based on dynamical aspects we have obtained that the HTN model has too slow diffusion although results obtained for both the molecular conformation and the structure were in reasonable agreement with experiment. We have found quite a good agreement for the self-diffusion coefficients between the OPLS-like models and experiments, especially for J and JMOD. The JMOD model, however, gives an unreasonable intramolecular conformation. The results obtained for the D coefficients as a function of the model used suggest a coupling between intramolecular motions and self-diffusion, in agreement with previous studies, rather than a dependence on the mean molecular conformation (molecular shape) or differences in the intermolecular hydrogen bonding patterns.

ACKNOWLEDGMENTS

We thank Dr. F. Hutchinson for useful comments and suggestions. This work has been supported by DGICYT (Grant No. PB96-0170-C03) and by CIRIT (Grants No. 1997SGR-00149 and No. 1999SGR-00146).

[1] B. M. Ladanyi and M. S. Skaf, Annu. Rev. Phys. Chem. **44**, 335 (1993).
[2] J. A. Padró, L. Saiz, and E. Guàrdia, J. Mol. Struct. **416**, 243 (1997).
[3] L. Saiz, J. A. Padró, and E. Guàrdia, J. Phys. Chem. B **101**, 78 (1997).
[4] L. Saiz, J. A. Padró, and E. Guàrdia, Mol. Phys. **97**, 897 (1999).
[5] L. Saiz, E. Guàrdia, and J. A. Padró, J. Chem. Phys. **113**, 2814 (2000).
[6] G. Widmalm and R. W. Pastor, J. Chem. Soc., Faraday Trans. **88**, 1747 (1992).
[7] H. Hayashi, H. Tanaka, and K. Nakanishi, Fluid Phase Equilibria **104**, 421 (1995).
[8] H. Hayashi, H. Tanaka, and K. Nakanishi, J. Chem. Soc., Faraday Trans. **91**, 31 (1995).
[9] P. I. Nagy, W. J. Dunn III, G. Alagona, and C. Ghio, J. Am. Chem. Soc. **113**, 6719 (1991).
[10] P. I. Nagy, W. J. Dunn III, G. Alagona, and C. Ghio, J. Am. Chem. Soc. **114**, 4752 (1992).
[11] G. Alagona and C. Ghio, J. Mol. Struct.: THEOCHEM **254**, 287 (1992).
[12] R. W. W. Hooft, B. P. van Eijck, and J. Kroon, J. Chem. Phys. **97**, 6690 (1992).
[13] R. W. W. Hooft, B. P. van Eijck, and J. Kroon, J. Chem. Phys. **97**, 3639 (1992).
[14] O. Bastiansen, Acta Chem. Scand. (1947-1973) **3**, 415 (1949).
[15] J.-Y. Huot, E. Battistel, R. Lumry, G. Villeneuve, J.-F. Lavallee, A. Anusiem, and C. Jolicoeur, J. Solution Chem. **17**, 601 (1988).
[16] G. Douheret, A. Pal, H. Hoiland, O. Anowi, and M. I. Davies, J. Chem. Thermodyn. **23**, 569 (1991).
[17] B. P. Jordan, R. J. Sheppard, and S. Szwarnowski, J. Phys. D **11**, 695 (1978).
[18] A. C. Kumbharkhane, S. M. Puranik, and S. C. Mehrotra, J. Solution Chem. **21**, 201 (1992).
[19] A. Lux and M. Stockhausen, Phys. Chem. Liq. **26**, 67 (1993).
[20] F. F. Hanna, A. Ghoneim, G. Turky, G. Klages, and M. Stockhausen, J. Mol. Liq. **69**, 133 (1996).
[21] S. v. Hornhardt, M. Stockhausen, H. Herba, J. Jadzyn, G. Czechowski, and B. Zywucki, J. Mol. Liq. **69**, 201 (1996).
[22] S. Takahashi and N. Nishi, Bull. Chem. Soc. Jpn. **68**, 539 (1995).
[23] P. Buckley and P. A. Giguère, Can. J. Chem. **45**, 397 (1967).
[24] H. Takeuchi and M. Tasumi, Chem. Phys. **77**, 21 (1983).
[25] H. Frei, T.-K. Ha, R. Meyer, and Hs. H. Günthard, Chem. Phys. **25**, 271 (1977).
[26] H. Matsuura and T. Miyazawa, Bull. Chem. Soc. Jpn. **40**, 85 (1967).
[27] H. Matsuura, M. Hiraishi, and T. Miyazawa, Spectrochim. Acta A **28**, 2299 (1972).
[28] W. K. Busfield, M. P. Ennis, and I. J. McEwen, Spectrochim. Acta A **29**, 1259 (1973).
[29] P.-E. Kristiansen, K.-M. Marstokk, and H. Mollendal, Acta. Chemica Scandinavica A **41**, 403 (1987).
[30] G. Chidichimo, D. Imbardelli, M. Longeri, and A. Saupe, Mol. Phys. **65**, 1143 (1988).
[31] S. R. Salman, R. D. Farrant, P. N. Sanderson, and J. C. Lindon, Magn. Reson. Chem. **31**, 585 (1993).
[32] W. Caminati and G. Corbelli, J. Mol. Spectrosc. **90**, 572 (1981).
[33] F. A. J. Singelenberg and J. H. van der Maas, J. Mol. Struct. **243**, 111 (1991).
[34] M. Forsyth and D. R. MacFarlane, J. Phys. Chem. **94**, 6889 (1990).
[35] V. Crupi, M. P. Jannelli, S. Magazu, G. Maisano, D. Majolino, P. Migliardo, and D. Sirna, Mol. Phys. **84**, 645 (1995).
[36] R. Buchner and co-workers (private communication).
[37] K. G. R. Pachler and P. L. Wessels, J. Mol. Struct. **6**, 471 (1970).
[38] A. K. Soper, Faraday Discuss. **103**, 41 (1996).
[39] P. S. Salmon and S. E. Okan (private communication).
[40] P. B. Lond, P. S. Salmon, and D. C. Champeney, J. Am. Chem. Soc. **113**, 6420 (1991); S. E. Okan and P. S. Salmon, J. Phys.: Condens. Matter **6**, 3839 (1994); S. E. Okan, P. S. Salmon, D. C. Champeney, and I. Petri, Mol. Phys. **84**, 325 (1995); S. E. Okan and P. S. Salmon, *ibid.* **85**, 981 (1995).
[41] P.-G. de Gennes, *Scaling Concepts in Polymer Physics* (Cornell University Press, Ithaca, 1979).
[42] W. L. Jorgensen, J. Phys. Chem. **90**, 1276 (1986).
[43] *CRC Handbook of Chemistry and Physics*, 4th ed. (CRC, New York, 1994).
[44] L. Verlet, Phys. Rev. **159**, 98 (1967).
[45] H. J. C. Berendsen, J. P. M. Postma, W. F. van Gunsteren, A. DiNola, and J. R. Haak, J. Chem. Phys. **81**, 3684 (1984).
[46] J.-P. Ryckaert, G. Ciccotti, and H. J. C. Berendsen, J. Comput. Phys. **23**, 327 (1977).
[47] M. P. Allen and D. J. Tildesley, *Computer Simulation of Liquids* (Oxford University Press, Oxford, 1987).
[48] D. Frenkel and B. Smit, *Understanding Molecular Simulation* (Academic, London, 1996).
[49] However, as stated by O. Bastiansen (Ref. 14), experimental data could also be interpreted if an oscillation about the C–C bond with an amplitude of approximately 75° with the *trans* conformation as the equilibrium position is assumed.
[50] S. Reiling, J. Brickmann, M. Schlenkrich, and P. A. Bopp, J. Comput. Chem. **17**, 133 (1996).
[51] T.-K. Ha, H. Frei, R. Meyer, and Hs. H. Günthard, Theor. Chim. Acta **34**, 277 (1974).
[52] B. J. Costa Cabral, L. M. P. C. Albuquerque, and F. M. S. Silva Fernandes, Theor. Chim. Acta **78**, 271 (1991).
[53] M. A. Murcko and R. A. DiPaola, J. Am. Chem. Soc. **114**, 10010 (1992).
[54] J. Almlöf and H. Stymne, Chem. Phys. Lett. **33**, 118 (1975).
[55] S. A. Vázquez, M. A. Ríos, and L. Caballeira, J. Mol. Struct. **6**, 471 (1970).
[56] C. van Alsenoy, L. van den Enden, and L. Schäfer, J. Mol. Struct.: THEOCHEM **108**, 121 (1984).
[57] L. Radom, W. A. Lathan, W. J. Hehre, and J. A. Pople, J. Am. Chem. Soc. **95**, 693 (1973).
[58] F. Podo, G. Némethy, P. L. Indovina, L. Radics, and V. Viti, Mol. Phys. **27**, 521 (1974).

[59] Experimental results using this technique in ethylene glycol solutions show the following values of the fraction of *gauche* isomers in several solvents (Ref. 37): 5% in $(C_2H_5)_3N$ lead to 0.80−0.77 fraction of *gauche* isomer, 20% in $(C_2H_5)_3N$ lead to 0.81−0.76 fraction of *gauche* isomer, 7%−12% in dioxane−d_8 lead to 0.86−0.84 fraction of *gauche* isomer, 20% in CH_3COCH_3 lead to 0.83−0.81 fraction of *gauche* isomer, 20% in acetonitrile lead to 0.87−0.85 fraction of *gauche* isomer, 20% in heavy water lead to a 0.88−0.87 fraction of *gauche* isomer, whereas a 0.86 fraction of *gauche* isomer was found in the neat liquid.

[60] In EPMC calculations, the simulation is driven by a set of interatomicpotential energy functions which are perturbed continuously throughout the simulation in such a way that the calculated distribution functions reproduce the measured distribution functions.

[61] L. Saiz, J. A. Padró, and E. Guàrdia (preprint).

[62] H. J. Bohm, I. R. McDonald, and P. A. Madden, Mol. Phys. **49**, 347 (1983).

[63] Values for the distances are those used in the simulations.

[64] N. Chandrasekhar and P. Krebs, J. Chem. Phys. **112**, 5910 (2000).

[65] J. H. R. Clarke and D. Brown, Mol. Phys. **58**, 815 (1986).